

**Cite this article as:** Li Jianhua, Zhang Cheng, Feng Ruicheng, et al. Multiscale Model for Crack Propagation of  $\gamma/\gamma$  Interface in  $\gamma$ -TiAl Alloy Based on Cohesive Zone Model[J]. Rare Metal Materials and Engineering, 2021, 50(05): 1617-1625.

ARTICLE

# Multiscale Model for Crack Propagation of $\gamma/\gamma$ Interface in $\gamma$ -TiAl Alloy Based on Cohesive Zone Model

Li Jianhua<sup>1,2</sup>, Zhang Cheng<sup>1</sup>, Feng Ruicheng<sup>1,2</sup>, Wang Junjun<sup>3</sup>, Wang Maomao<sup>1</sup>, Li Haiyan<sup>1,2</sup>, Qi Yongnian<sup>1</sup>, Rui Zhiyuan<sup>1,2</sup>

<sup>1</sup> School of Mechanical and Electrical Engineering, Lanzhou University of Technology, Lanzhou 730050, China; <sup>2</sup> Key Laboratory of Digital Manufacturing Technology and Application, Ministry of Education, Lanzhou University of Technology, Lanzhou 730050, China; <sup>3</sup> LS Casting and Forging Branch, Lanzhou LS Group Co., Ltd, Lanzhou 730050, China

**Abstract:** The multiscale model was established to predict the crack propagation behavior of  $\gamma$ -titanium aluminide (TiAl) alloys. The constitutive parameters of the cohesive zone model (CZM) of true twin (TT)  $\gamma/\gamma$  interface were obtained by molecular dynamics (MD). The mesoscopic model of polycrystalline  $\gamma$ -TiAl was generated via Voronoi method, and the CZM constitutive parameters were coupled into the model. The corresponding critical stress fracture diagrams with non-defect, blunt crack and blunt crack+central cavity defect were obtained. Furthermore, the polycrystalline model and the overall force-displacement curve were averaged by the geometric similarity, and the damage mechanism of  $\gamma$ -TiAl alloy was analyzed. At the same time, the macroscopic finite element model (FEM) was constructed according to the homogeneous material hypothesis. A cohesive region was built in the interested crack area, and then the force-displacement relationship and fracture toughness of  $\gamma$ -TiAl alloy was obtained through the FEM simulation of the compact tensile specimen. Finally, the results show that the comparison between the crack propagation behavior obtained from the macroscale finite element simulation and the experimental results proves the validity of the multiscale model. The defects have a significant sensitivity on the strength of the entire near- $\gamma$  structure when the ratio of grain is the same, and meanwhile this analysis method can effectively connect various scales and predict the growth of cracks.

**Key words:**  $\gamma$ -TiAl alloy; multiscale model; Voronoi tessellation; FEM-CZM

TiAl alloys have excellent high-temperature mechanical properties, low density, high stiffness constituents and corrosion resistance performance, so they are widely used in the aerospace industry<sup>[1,2]</sup>. A lot of researches were performed to investigate the properties and failure of TiAl alloys at microscale and macroscale. For example, Booth et al<sup>[3]</sup> studied the change of fracture toughness under the brittle-ductile transition in  $\gamma$ -TiAl single crystals. Guo et al<sup>[4]</sup> discussed the influence of microstructure on the physical properties and internal stress-strain of a TiAl-based alloy. After studying the properties of TiAl, the research on its failure in aero-engine applications also attracts so much attention.

The crack is an essential factor resulting in the failure of TiAl alloy<sup>[5]</sup>, which involves people's life and property safety,

so it is necessary to explore the mechanism of the crack propagation of TiAl alloy. Wu et al<sup>[6]</sup> investigated the plastic deformation and initiation of various surface defects of single-crystal  $\gamma$ -TiAl along [001] uniaxial-tensile direction by molecular dynamics (MD). Kong et al<sup>[7]</sup> studied the factors affecting the ductility of TiAl-based alloys at room temperature. Iqbal et al<sup>[8]</sup> found that the crack nucleation at the  $\gamma/\gamma$  and  $\alpha_2/\gamma$  interfaces and inside the  $\gamma$  phase always precedes the intense local elastic deformation. However, those literatures only involved the problems at different scales. Moreover, the destruction and failure of materials are caused by micro defects extending to the larger scale<sup>[9]</sup>. Therefore, a simulation method considering multiscale can be used to comprehend the mechanism of damage in TiAl alloys more systematically.

Received date: October 08, 2020

Foundation item: National Natural Science Foundation of China (52065036, 51865027); Hongliu First-class Disciplines Development Program of Lanzhou University of Technology

Corresponding author: Feng Ruicheng, Ph. D., Associate Professor, School of Mechanical and Electrical Engineering, Lanzhou University of Technology, Lanzhou 730050, P. R. China, E-mail: postfeng@lut.edu.cn

Copyright © 2021, Northwest Institute for Nonferrous Metal Research. Published by Science Press. All rights reserved.

The modeling method can organically correlate the physical properties and geometric parameters of cracks at different scales from qualitative and quantitative aspects. Multiscale methods with the microscale and macroscale can predict the failure of materials effectively<sup>[10,11]</sup>. Fig. 1 shows the structure and characterization of materials at different scales. MD was applied to study the microstructure ( $10^{-9}$  m), the Voronoi method was used at the mesoscale ( $10^{-6}$  m), and the finite element model (FEM) was used to simulate the macroscale ( $10^{-3}$  m). Then the characteristics of the material were analyzed comprehensively. Knezevic et al<sup>[12]</sup> applied the crystal slip of dislocation and critical activation stress of deformation twins in the polycrystalline plastic model to predict several constitutive responses. Sato<sup>[13]</sup> utilized the stress state obtained from the crack initiation in the macroscopic uniaxial tensile plate to analyze the microscopic periodic unit-cell (PUC). Bridging scales based on appropriate coupling parameters, such as critical activation stress and stress-strain state, can combine the microscopic constitutive and macroscopic phenomena better.

To study the fracture process, the classical theory provides a computational method and a model for the aspect of energy and force<sup>[14]</sup>. The theory involves some relevant mechanical parameters, such as energy release rate  $G$ ,  $J$ -integral, and stress intensity factor (SIF)  $K$ . Because the crack tip is the stress bearing point, the energy release rate is the largest at the crack tip. The energy analysis method and related mechanical parameters were used to describe the stress field near the crack tip region when it comes to the situation that the stress field cannot be explained by traditional fracture theory. For instance, some parts fail without any apparent warning. The reason is that the formation and propagation of microcracks are challenging to observe at the structure level.

Due to the complexity of the crystal interface's mechanical properties and the constraints of experimental technique, it is challenging to observe the dynamic fracture process of the polycrystalline TiAl alloy and establish a mechanical model. Besides, the microcrack propagation along the crystal occurs at the interface level. Recently, the constitutive structure of multiscale fracture simulation has been studied in detail,

which provides a better description of the generation and propagation of macrocracks<sup>[15,16]</sup>. The cohesive zone model (CZM) is a constitutive model used to simulate the production and growth of cracks. In constitutive relation, the traction-separation (T-S) law mainly controls the crack growth<sup>[17]</sup>. The relation obtained from the atomic simulations was used to study the damage evolution of the grains and macro fracture. Hence, a multiscale modeling approach emerges to connect atomic-level damage mechanisms with structural failure. Lyu et al<sup>[18]</sup> developed a layered high-order multiscale cohesive zone model (MCZM) to simulate the dynamic propagation of cracks in the crystal, and showed that the crack propagation velocity is consistent with the corresponding dynamic simulation. Xu et al<sup>[19]</sup> provided a hybrid multiscale method linking the micro and mesoscopic scales to investigate the fracture behavior of brittle body-centered cubic (bcc) Fe. These studies showed that the method of coupling multiple scales to the cohesion model is feasible. However, few studies investigate the effect of the multiscale and polycrystalline composition of  $\gamma$ -TiAl alloys on crack growth. In this research, the T-S parameters of CZM of the true twin (TT) interface were extracted from a microscopic atomic simulation and applied to the polycrystalline fracture model of  $\gamma$ -TiAl. The strength situation of different defects of grains and the corresponding relationship of damage under polycrystals were obtained. Verification of the role of bridging parameters at the scale of the polycrystalline interface was given, and the force-displacement relationship was obtained to illustrate the initiation and propagation of cracks. Furthermore, the fracture toughness was obtained through the simulation in the macro model. The results were compared with the experiment results to illustrate the situation of the model.

## 1 Method and Modeling

### 1.1 Crack model of CZM

CZM was applied to simulate the interface crack. The concept was firstly proposed by Dugdale<sup>[20]</sup> and Barenblatt<sup>[21]</sup>. Because the existing stress field is singular at the crack tip, the

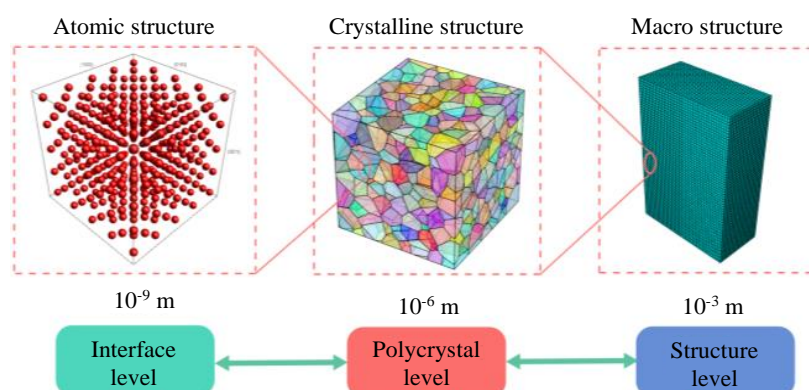


Fig.1 Schematic diagram of modeling levels at different scales

phenomenon can be avoided by the cohesive model. The constitutive model is expressed in Fig.2 for researching the initiation and propagation of cracks in the materials at different scales. Wang et al<sup>[22]</sup> simulated the uniaxial tension of pipeline steel in the CZM and obtained two critical relations between load-displacement and crack tip open angle (CTOA)-fracture speed, which effectively predicted the crack growth.

The purpose of the multiscale analysis of material deformation characteristics is to build qualitative and quantitative relationships between physical variables and geometrical parameters at different scales. In order to study the fracture behavior of  $\gamma$ -TiAl, a serial multiscale method was applied to analyze the multiscale coupling of microscale, mesoscale and macroscale across the continuum theory. Therefore, the CZM constitutive parameter can be used in the coupling relationship among multiple scales to predict the initiation and propagation of cracks. For the definition of the CZM parameters, the cohesion force is equivalent to the damage stress in Fig.2. The initial damage stress value should reach  $T_{max}$ , and the failure displacement (separation) is  $\delta_{init}$  in the bilinear curve when the cohesion zone begins to break. Moreover, the fracture energy  $G_{IC}$  of the cohesion zone also reaches the largest value when the failure displacement reaches the maximum  $\delta_{fail}$ . At the same time, the cohesion zone was wholly damaged and separated, while the crack continued to break along the next zone.

## 1.2 CZM parameters of microstructure

In the grain fracture simulation, the  $\gamma$  interface has three

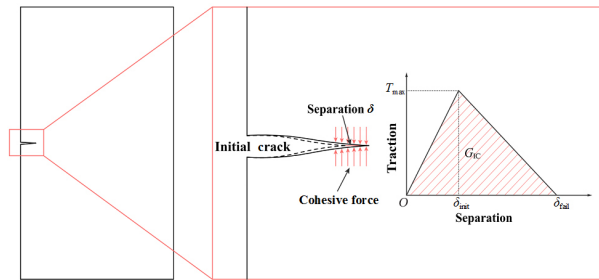


Fig.2 Schematic diagram of cohesive zone model

types: true-twin, rotational boundary (RB) and pseudo-twin (PT) with the same orientation. Among these interfaces, it has better physical properties since TT interface requires greater separation work. Furthermore, because of the modulus misfit in RB and PT samples, the TT data were used to build the  $\gamma$ -TiAl polycrystalline model. To simulate the fracture process of fine-grain, a microscopic simulation of the TT interface was established, as shown in Fig.3. The size of the entire MD model was 49.0 nm×55.4 nm×2.2 nm, and the total number of atoms was 385 600. The crystal direction was along the orientation of  $X[11\bar{2}]$ ,  $Y[111]$ ,  $Z[1\bar{1}0]$ . At the same time, a defective model was set up for comparison. The fracture process of the model includes the stretch along  $Y$ -direction with a strain rate of  $2 \times 10^8 \text{ s}^{-1}$ . To prevent the atoms from moving along  $X$ -direction, a free boundary condition was applied. The entire model simulates 1 000 000 steps under the micro-canonical ensemble (NVE) with periodic boundary conditions along  $X$ ,  $Z$  direction and shrink-wrapped boundary condition along  $Y$  direction (psp).

After MD simulates the fracture of TT interface, it is necessary to extract the T-S parameters at the interface. As shown in Fig.3, the T-S region was defined and divided into the top area (T) and the bottom area (B). The T-S relationship can be derived by analyzing the average atomic stress and relative displacement in this region. For the non-defect model, the model with blunt crack and blunt crack+center void can also be helpful for comparison and analysis of mesoscale and macroscale effects of defects.

## 1.3 Fracture application of Voronoi model

Voronoi tessellation is used in metallography and crystallography<sup>[23]</sup>. The method constructs a polycrystalline constitutive model of copper<sup>[24]</sup>, which analyzes the size effect under different grain sizes and studies the impact of grain orientation and its evolution during plastic deformation. The Voronoi tessellation location is random with a certain number of discrete sites  $S$  (Voronoi seeds) and the grain boundaries which form the zone  $X$  with the shortest distance. It has the following relationship with the Voronoi tessellation region  $\Omega_i$ , which is given as follows<sup>[25]</sup>:

$$\Omega_i = \{x \in X | d(P_i, x) < d(P_j, x)\}, i \neq j \quad (1)$$

where  $X$  is a set of Euclidean distance functions  $d$ ; the distance from the  $P_i$  site of Voronoi cell to the  $X$  set is shorter

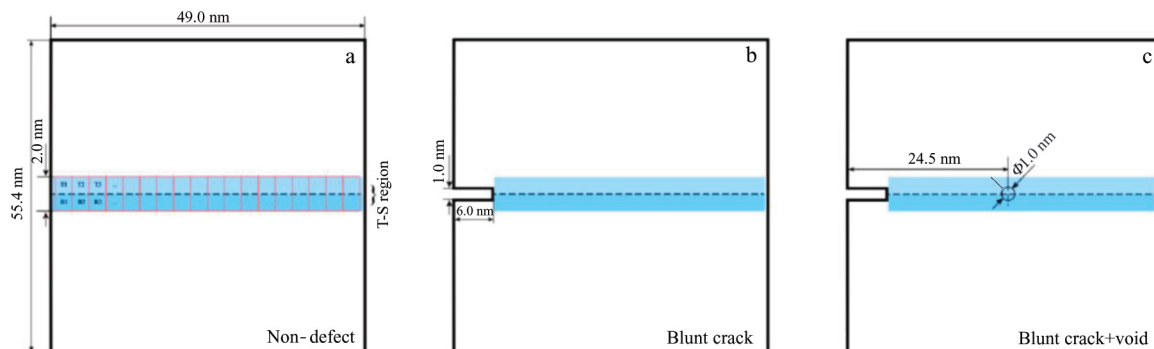


Fig.3 Schematic diagrams of non-defect (a), blunt crack (b), and blunt crack+center void (c) MD models

than the relative distance from  $P_j$  site to  $X$  set; the  $S$  in  $\Omega_i$  is often disjoint in the model. An example of the two-dimensional Voronoi tessellation is shown in Fig.4, which generates the desired polycrystalline model.

In order to accurately simulate polycrystalline fracture, the elastic constants obtained from the experiments<sup>[26,27]</sup> are listed in Table 1. According to the research of polycrystalline fracture process of the  $\gamma$ -TiAl, the influence of microscopic defects on polycrystalline can be clarified. The initial mesoscopic structure of  $\gamma$ -TiAl<sup>[28]</sup> is shown in Fig.5a.

The crystal orientation along  $\langle 1\bar{1}0 \rangle$  is different from that along  $\langle 01\bar{1} \rangle$  in the  $L1_0$  structure. The entire domain boundaries of the TT often show  $180^\circ$  rotation faults. The corresponding  $\gamma/\gamma$  interface only has three symmetrical interface slip orientations:  $[1\bar{1}0]$ ,  $[10\bar{1}]$  and  $[01\bar{1}]$ . This interface only changes in the stacking order of the parent  $L1_0$  structure. Based on the volume fraction and crystal orientation of the grains, a polycrystalline model of  $40\text{ }\mu\text{m} \times 40\text{ }\mu\text{m}$  was constructed to simulate the crystalline fracture of  $\gamma$ -TiAl alloy along all three crystal directions. The relationship between the area distribution of each grain and the number of grains is shown in Fig.5b.

1.4 Establishment of macro-fracture model

For the purpose of verifying the correctness of the micro bridge to the mesoscopic model, a cohesive element with a ze-

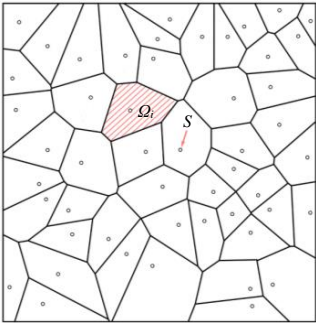


Fig.4 Schematic diagram of Voronoi tessellation

ro thickness was used to simulate the cracks in the macroscale finite element system. The whole model is shown in Fig. 6, with a width of  $500\text{ }\mu\text{m}$  and a length of  $480\text{ }\mu\text{m}$ . Furthermore, the notch width ( $W$ ) was  $40\text{ }\mu\text{m}$  in the compact tensile (CT) specimen, and the length of the pre-crack ( $a$ ) and the dimension of cohesion region were  $200\text{ }\mu\text{m}$  and  $200\text{ }\mu\text{m} \times 40\text{ }\mu\text{m}$ , respectively. The load was applied to the upper circle of the specimen along the positive  $Y$ -direction, and the lower circle was fixed. The diameter of the circle was  $100\text{ }\mu\text{m}$ . The uniaxi-

Table 1 Elastic constants and related parameters of TiAl alloys

$C_{11}/\text{GPa}$	$C_{12}/\text{GPa}$	$C_{13}/\text{GPa}$	$C_{33}/\text{GPa}$	$C_{44}/\text{GPa}$	$C_{66}/\text{GPa}$	$K/\text{GPa}$	$G/\text{GPa}$	$E/\text{GPa}$	$\nu$
186	72	74	176	101	77	110	74	181.5	0.23

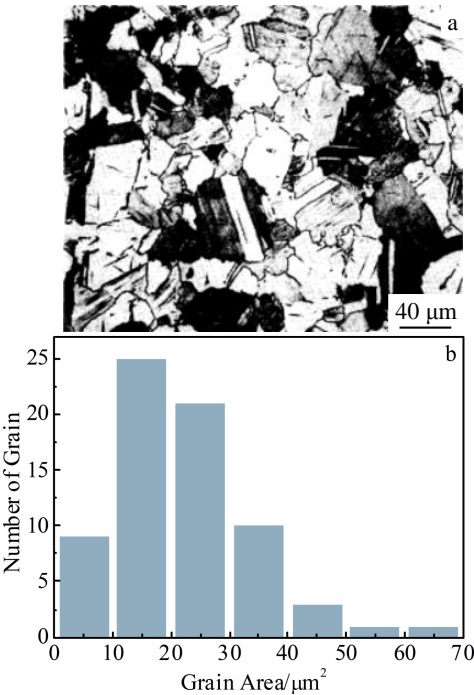


Fig.5 Initial microstructure of  $\gamma$ -TiAl reproduced from experiment<sup>[28]</sup> (a); distribution results of grain area (b)

al tensile load was applied at a constant displacement under the plane strain conditions, and the final simulation result was obtained.

In the decohesion process, the maximum nominal stress criterion determines the crack damage evolution criterion, and the parameters convert when the geometric thickness is 1 in the FEM. Therefore, the tangential damage stress and fracture energy were consistent with the parameters in the normal direction. In the grid division, it should be refined as much as possible in the expected fracture area. Other unbreakable areas should be divided into coarse meshes.

2 Results and Discussion

2.1 T-S parameters of crack propagation

In order to analyze the crack propagation influence of different simulation styles, the MD simulation of the twin interface at 300 K is shown in Fig.7, which shows the initiation stage and the crack propagation stage after the tensile stress increases. In Fig. 7, the gray contrast patches appear after stretching due to the accumulation and disorder of atoms. Furthermore, it can be found that the holes appear at the twin interface, and gradually form cracks as the tensile stress increases in Fig.7a. In Fig.7b and 7c, the initiation cracks are near the defect, and a regular path forms when the blunt crack starts to expand. The data obtained from the T-S region transform into a scatter plot, and a bilinear image synthesizes, as shown in Fig.8. In



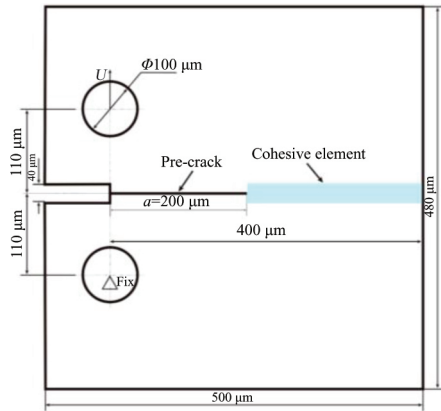


Fig.6 Schematic diagram of CT specimen for FEM modeling

addition, the bilinear image transforms into a related parameter by the concept of the cohesive parameter in Fig.2.

The corresponding cohesion parameters are obtained when the T-S region is set in the simulation model, and these parameters are listed in Table 2. It can be observed that the tensile stress is the largest when there are no defects at the twin boundary. The maximum separation displacement of the entire model is also the largest, proving that more fracture energy is needed to generate cracks as there are no defects at the interface. The energy required for the crack is smaller when there are defects at the interface, making the crack propaga-

tion easier.

## 2.2 Intergranular fracture of polycrystalline $\gamma$ -TiAl

The results show the critical stress cloud diagram in Fig.9. For the gamma phase structure, an intergranular fracture occurs at the interface  $\gamma/\gamma$  during the stretching process in which the grain number is 70. It can be observed that the crack initiation is faster when the cohesive force parameters of the defect model are applied to the model. The above situation shows that the microscopic defects cause the interface sensitivity of mesoscopic polycrystalline and the first interface crack occurs earlier. Afterward, as the load increases, the crack continues to grow along with the interface and forms the main crack. At the crack initiation stage, as shown in Fig.9, it can be seen that the high-stress areas are initially at the intersection of the interface. Stress concentrations occur at the intersection of the interface, and then the new cracks may emerge. Moreover, with the crack initiation and continuous growth at the grain boundary, microcracks nucleate at the interface and propagate along the grain boundary under the load along [001] direction. The crack length is greater than the characteristic size of the structure, namely the average grain size in the near- $\gamma$  structure, and the microcrack eventually forms the main crack. The stress concentration at the interface of the original high-stress zone is released. Along with continuous propagation, the high-stress zone exists at the crack tip of the main crack. Eventually, the expansion of the main crack leads to the failure of the entire structure.

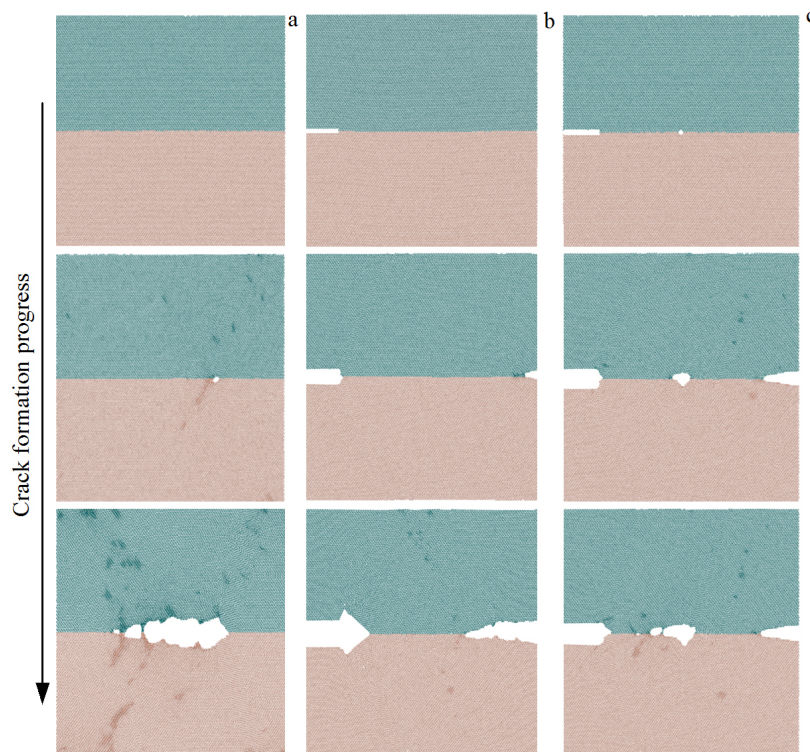


Fig.7 Different fracture processes in MD simulation: (a) non-defect, (b) blunt crack, and (c) blunt crack+void defect

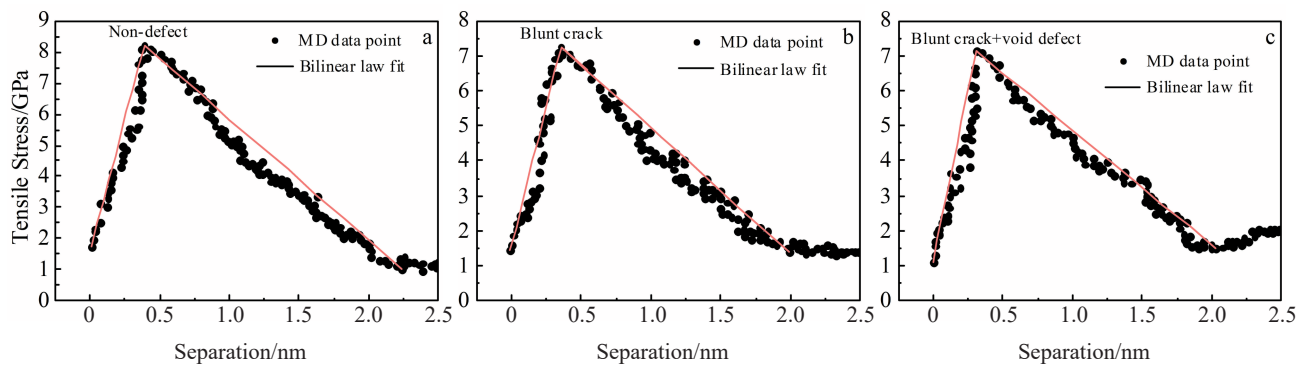


Fig.8 T-S results of non-defect (a), blunt crack (b), and blunt crack+void defect (c) fracture processes

It can be found from Fig.9 that the main crack is perpendicular to the loading direction, accompanied by the initiation of some microcracks. With the increase of load, cracks also appear on the other side of the TiAl alloy and expand to the center. When the load causes a brittle fracture, the discontinuous microcracks gradually overlap together, which breaks the model. The edge cracks can also be observed when the simulation style is non-defect in Fig.9a. Besides, the Mises stress near the main crack gradually decreases as the defects at the interface increase, as shown in Fig.9b and 9c. It shows that the critical stress required for crack propagation is gradually smaller.

According to the observed polycrystalline fracture process in Fig.10, the crack initiation is highly sensitive to the crystalline interface structure during the crack initiation process. The inability to quantitatively describe the crystal structure makes it difficult to predict the occurrence of cracks. However, after the formation of the primary crack in the structure equivalent to the characteristic size of the grain, the local stress state of the crack tip is the main factor which dominates the crack

propagation. The load value is a reaction force on the bottom surface, which indicates that its strength improves with the variation of interface situation. Furthermore, it can be inferred that the grain structure and local failure mode are different. In the end, the main crack propagates along the crystalline interface and eventually fails after the crack initiation.

2.3 Macroscopic fracture simulation

In Fig.11, the generated grid elements are CPE4R. In order to simulate the crack propagation as appropriately as possible, the mesh of the middle prefabricated crack attention area is refined. Moreover, the COH2D4 elements are applied to CPE4R meshes in the refined area (Fig.6). In the coarse grid region, the average size of all the CPE4R elements is about 15  $\mu\text{m}$ . The minimum size of the refined mesh in the crack concern area is 1  $\mu\text{m}$ . The constitutive parameters obtained from the MD simulation can be applied to the refined grid in the middle region. The parameters include the initial damage stress  $\sigma$ , initial stiffness  $K$  and fracture energy  $G_{\text{ic}}$ . These parameters can be extracted from T-S curve, as shown in Fig.2.

Table 2 Parameters of bilinear curve in directions<sup>[9]</sup>

Simulation style	Damage stress/GPa	Maximum separation/nm	Stiffness/ $\times 10^7 \mu\text{N} \cdot \mu\text{m}^{-3}$	Fracture energy/ $\text{J} \cdot \text{m}^{-2}$
Non-defect	8.08	2.658	2.38	10.74
Blunt crack	7.35	2.536	2.27	9.32
Blunt+void defect	7.29	2.417	2.21	8.81

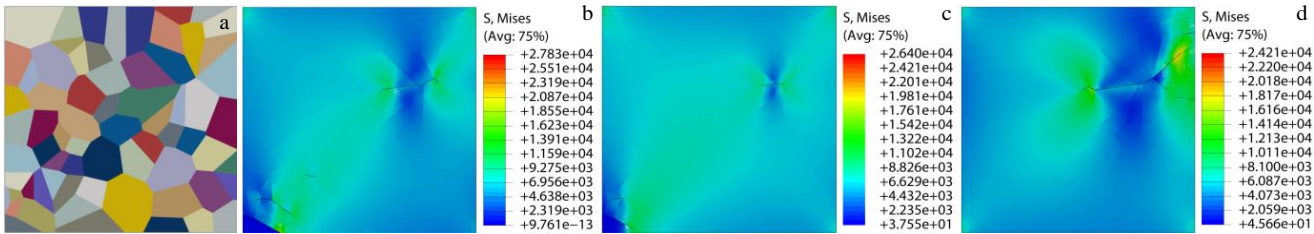


Fig.9 Single-phase TiAl polycrystalline figure (a) and critical stress cloud diagrams for fractures with different defects: (b) non-defect, (c) blunt crack, and (d) blunt crack+void defect

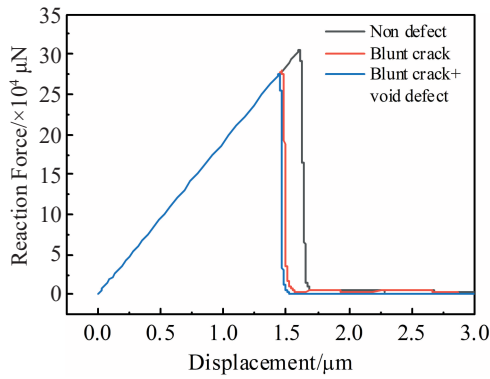


Fig.10 Relationship between reaction force and displacement for different simulation types

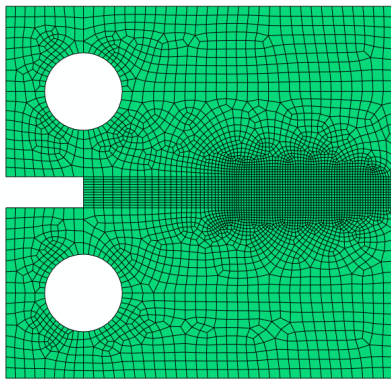


Fig.11 Finite element meshes for macroscale model

It can be observed that the crack propagates along the area in Fig. 12. The crack propagation path is single and smooth. The type of expansion is roughly consistent with the open type expansion. The crack propagation path is fully developed when the loading displacement is 7  $\mu\text{m}$ , and the stress field is also expanded. Meanwhile, in Fig. 12a, the crack length is greater than that in Fig. 12b and 12c. The stress tip area is compared with the previous state of the stress field distribution, and the gradient is similar, indicating that during the fracture

process, the crack tip is the primary bearing area.

The fracture under the cohesive constitutive parameters of different defects is simulated to reveal the effect on the macroscopic crack propagation. The tensile failure model under different defects is shown in Fig. 13a. In the early elastic stage, the entire CT specimen exhibits the same behavior due to the presence of prefabricated cracks. As the model continues to be stretched, the crack propagates from the preset crack to the cohesive region. It can be observed from Fig. 13a that the maximum force value of the model locates basically at the initial failure stage of the cohesive zone, and the stress at the crack tip at the same time is also the maximum during the fracture process. It is found that the damaging force decreases during the crack propagation process. The elastic response before failure is smooth after the initial stage. According to the theory of linear elastic fracture mechanics, the stress intensity factor (SIF)  $K_I$  at the crack tip is expressed as follows<sup>[29]</sup>:

$$K_I = \frac{F}{B\sqrt{W}} f\left(\frac{a}{W}\right) \quad (2)$$

$$f\left(\frac{a}{W}\right) = \frac{2 + \sqrt{\frac{a}{W}}}{\left(1 - \frac{a}{W}\right)^{3/2}} \left[ 0.886 + 4.64\left(\frac{a}{W}\right) - 13.32\left(\frac{a}{W}\right)^2 + 14.72\left(\frac{a}{W}\right)^3 - 5.60\left(\frac{a}{W}\right)^4 \right] \quad (3)$$

where  $F$  is a critical tensile force;  $B$  is the specimen thickness. The two-dimensional plane strain is applied during the FEM investigation, so the thickness effect is ignored, and the specimen thickness  $B$  is 1  $\mu\text{m}$ .

The force-displacement parameters are obtained from the FEM simulation and used to calculate SIF. The SIF depends on the critical stress when the material begins to fail. It can be seen that the range of fracture toughness is 14~16.5  $\text{MPa}\cdot\text{m}^{1/2}$  in Fig. 13b, while the corresponding value of the experiment is ~11.4  $\text{MPa}\cdot\text{m}^{1/2}$ <sup>[30]</sup>. The difference between the simulated and experimental SIF results is mainly caused by the difference between the near- $\gamma$  microscale structure and macroscale sample structure. According to the derivation of the simulation results, the strength of TT structure is greater than that of the near- $\gamma$  structure. Additionally, the simulation results are compared with the results of CT experiment of  $\gamma$ -TiAl alloy with

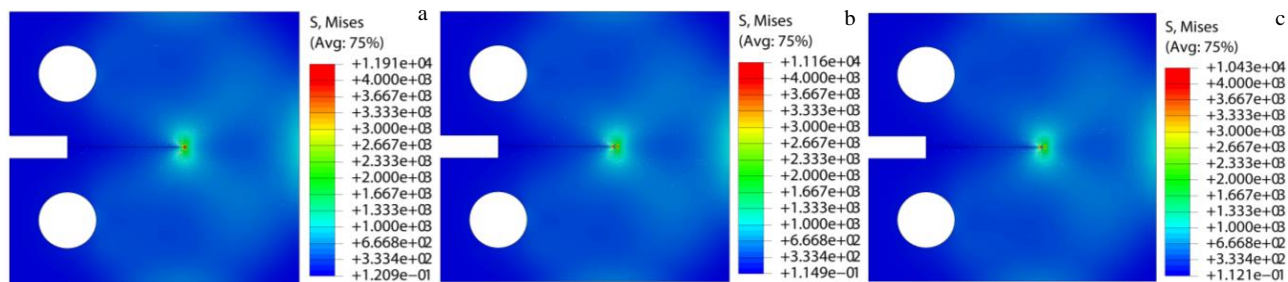


Fig. 12 Stress cloud diagrams for different macroscale fracture models: (a) non-defect, (b) blunt crack, and (c) blunt crack+void defect



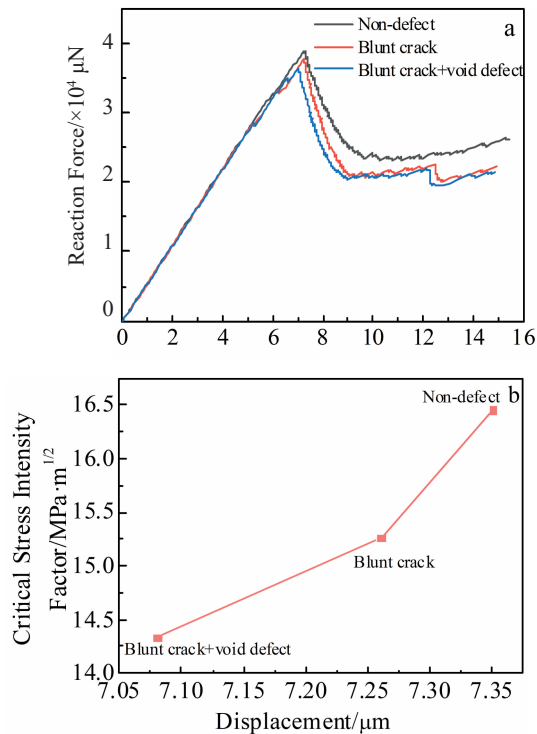


Fig.13 Relationship between reaction force and displacement (a) and calculated critical stress intensity factors (b) for multiscale simulation types

TT structure. It can further explain the influence of microscale interface on the macroscale fracture. The damage response for different defect types produced by the phase interface with uniform grain distribution is not much different when the number of grain is the same, but there is a certain tolerance in the accuracy of the model.

### 3 Conclusions

1) For the crystal structure of a  $\gamma$ -TiAl alloy, the presence or absence of defects have a significant influence on the strength of the entire near- $\gamma$  structure when the ratio of grain is the same. The blunt crack and void defect deforms more easily than the non-defect model does in TiAl grains at the elastic deformation stage.

2) It is feasible to establish the influence of micro-defects and macro-fracture based on the predictions related to the fracture toughness, which is helpful to understand the initiation and propagation of cracks from a multiscale perspective.

3) There are local changes in the structure related to the grain interface. Nevertheless, the damage response for different defect types produced by the phase interface with uniform grain distribution is not much different when the number of grains is the same. A better method to expand the cohesive zone model should be considered, because of the size effect of cohesion on the entire model, and there is a certain tolerance in the accuracy of the model.

### References

- Clemens H, Mayer S. *Materials Science Forum*[J], 2016, 879: 113
- Bewlay B P, Nag S, Suzuki A et al. *Materials at High Temperatures*[J], 2016, 33(3-4): 549
- Booth A S, Roberts S G. *Acta Materialia*[J], 1997, 45: 1045
- Guo F A, Ji V, Zhang Y G et al. *Materials Science and Engineering A*[J], 2001, 315(1-2): 195
- Bode B, Wessel W, Brueckner-Foit A et al. *Fatigue & Fracture of Engineering Materials & Structures*[J], 2016, 39(2): 227
- Wu H N, Xu D S, Wang H et al. *Journal of Materials Science & Technology*[J], 2016, 32(10): 1033
- Kong Dantao, Chen Ziyong. *Rare Metal Materials and Engineering*[J], 2003, 32(2): 81 (in Chinese)
- Iqbal F, Pyczak F, Neumeier S et al. *Materials Science and Engineering A*[J], 2017, 689: 11
- Zhang Y W, Cao L Q, Feng Y D et al. *Journal of Computational and Applied Mathematics*[J], 2017, 319: 460
- Zohdi T I. *Encyclopedia of Computational Mechanics Second Edition*[J], 2017: 1
- Wolf D, Yip S. *Materials Interfaces, Atomic-Level Structure and Properties*[M]. London: Chapman & Hall, 1992: 30
- Knezevic M, Beyerlein I J. *Advanced Engineering Materials*[J], 2018, 20(4): 1 700 956
- Sato Y, Okabe T, Higuchi R et al. *Advanced Composite Materials* [J], 2014, 23(5-6): 461
- Rafii-Tabar H, Hua L, Cross M. *Journal of Physics, Condensed Matter*[J], 1998, 10(11): 2375
- Zeng X, Li S. *Computer Methods in Applied Mechanics and Engineering*[J], 2010, 199(9-12): 547
- Matouš K, Kulkarni M G, Geubelle P H. *Journal of the Mechanics and Physics of Solids*[J], 2008, 56(4): 1511
- Scheider I, Brocks W. *Key Engineering Materials*[J], 2003, 251: 313
- Lyu D, Fan H, Li S. *Engineering Fracture Mechanics*[J], 2016, 163: 327
- Xu T, Stewart R, Fan J et al. *Engineering Fracture Mechanics* [J], 2016, 155: 166
- Dugdale D S. *Journal of the Mechanics and Physics of Solids*[J], 1960, 8(2): 100
- Barenblatt G I. *Advances in Applied Mechanics*[J], 1962, 7: 55
- Wang Y J, Ru C Q. *Engineering Fracture Mechanics*[J], 2016, 163: 55
- Okabe A, Boots B, Sugihara K et al. *Spatial Tessellations: Concepts and Applications of Voronoi Diagrams*[M]. New York: John Wiley & Sons, 2009: 43
- Peng L, Xu Z, Gao Z et al. *International Journal of Mechanical Sciences*[J], 2018, 138: 74
- Siersma D. *Geometry in Present Day Science*[J], 1999: 187
- Tanaka K, Okamoto K, Inui H et al. *Philosophical Magazine A*



- [J], 1996, 73(5): 1475
- 27 He Y, Schwarz R B, Migliori A et al. *Journal of Materials Research*[J], 1995, 10(5): 1187
- 28 Kim Y W. *Materials Science and Engineering A*[J], 1995, 192: 519
- 29 American Society for Testing and Materials. *ASTM E399-90*[S], 1990
- 30 Rao K T V, Kim Y W, Muhlstein C L et al. *Materials Science and Engineering A*[J], 1995, 192-193: 474

## 基于内聚力模型的 $\gamma$ -TiAl合金中 $\gamma/\gamma$ 界面裂纹扩展的多尺度模型

李建华<sup>1,2</sup>, 张成<sup>1</sup>, 冯瑞成<sup>1,2</sup>, 王军军<sup>3</sup>, 王茂茂<sup>1</sup>, 李海燕<sup>1,2</sup>, 祁永年<sup>1</sup>, 芮执元<sup>1,2</sup>

(1. 兰州理工大学机电工程学院, 甘肃 兰州 730050)

(2. 兰州理工大学数字制造技术与应用省部共建教育部重点实验室, 甘肃 兰州 730050)

(3. 兰州兰石集团有限公司 兰石铸锻分公司, 甘肃 兰州 730050)

**摘要:**通过建立多尺度模型预测 $\gamma$ -TiAl合金中裂纹的扩展行为。利用分子动力学(MD)建立了真孪晶(TT) $\gamma/\gamma$ 界面模型,得到了界面内聚力区域(CZM)的本构参数;采用Voronoi方法生成了多晶 $\gamma$ -TiAl合金介观模型,将CZM本构参数耦合到该模型中,得到了对应的不含缺陷、含钝裂纹和钝裂纹+中心空洞缺陷的临界应力断裂云图,利用几何相似性平均了多晶模型和整体裂纹拉伸关系曲线并分析了 $\gamma$ -TiAl合金的损伤机理;根据连续介质假说建立了宏观有限元模型(FEM),通过对紧凑拉伸试样模拟给出了力-位移曲线并得到了材料的断裂韧性。最后,将宏观有限元模拟得到的裂纹扩展行为与实验结果进行比较,验证了该模型的有效性。结果表明:在晶粒数比例相同的情况下,缺陷对整个近 $\gamma$ 结构的强度有着显著的敏感性,同时该多尺度方法可以有效地连接不同尺度并预测裂纹的扩展。

**关键词:** $\gamma$ -TiAl合金;多尺度模型;Voronoi镶嵌;有限元模型-内聚力

作者简介:李建华,男,1975年生,博士,副教授,兰州理工大学机电工程学院,甘肃 兰州 730050, E-mail: li\_jhlz@lut.edu.cn